ISSN 0036-0236, Russian Journal of Inorganic Chemistry, 2022, Vol. 67, No. 2, pp. 237–244. © The Author(s), 2022. This article is an open access publication.
Russian Text © The Author(s), 2022, published in Zhurnal Neorganicheskoi Khimii, 2022, Vol. 67, No. 2, pp. 248–256.

INORGANIC MATERIALS AND NANOMATERIALS

Effect of the Addition of Copper Particles on the Thermoelectric Properties of the $Ca_3Co_4O_{9+\delta}$ Ceramics Produced by Two-Step Sintering

A. I. Klyndyuk[a], *, E. A. Chizhova[a], R. S. Latypov[a], S. V. Shevchenko[a], and V. M. Kononovich[a]

[a] *Belarusian State Technological University, Minsk, 220006 Belarus*

**e-mail: klyndyuk@belstu.by*

Received July 7, 2021; revised August 2, 2021; accepted August 12, 2021

Abstract—Composite thermoelectric materials based on layered calcium cobaltite $Ca_3Co_4O_{9+\delta}$ doped with copper particles were synthesized by two-step sintering, and their microstructure, and electrotransport and thermoelectric properties were studied. It was determined that the introduction of copper particles into the ceramics improves their sinterability at moderate sintering temperatures ($T_{sint} \le 1273$ K), leading to a decrease in the porosity of the samples and an increase in their electrical conductivity and power factor, whereas the oxidation of copper to less conductive copper(II) oxide significantly decreases the electrical conductivity and power factor of the ceramics sintered at elevated temperatures ($T_{sint} \ge 1373$ K). The power factor is maximum for the $Ca_3Co_4O_{9+\delta}$ + 3 wt % Cu ceramic sintered at 1273 K (335 μW/(m K^2) at a temperature of 1100 K), which is by a factor of 2.3 higher than the power factor of the base material $Ca_3Co_4O_{9+\delta}$ with the same thermal history (145 μW/(m K^2) at 1100 K) and more than 3 times higher than the power factor of the $Ca_3Co_4O_{9+\delta}$ ceramic synthesized by the conventional solid-phase method.

Keywords: thermoelectric ceramics, two-step sintering, $Ca_3Co_4O_{9+\delta}$, copper, electrical conductivity, Seebeck coefficient, power factor

DOI: 10.1134/S0036023622020073

INTRODUCTION

Layered calcium cobaltite $Ca_3Co_4O_{9+\delta}$ has both high electrical conductivity σ and Seebeck coefficient *S*, and low thermal conductivity λ. Unlike conventional thermoelectric materials based on bismuth-lead selenides-tellurides, it is resistant in air at elevated temperatures and contains neither expensive, nor highly toxic components. Owing to this, this compound is considered as promising base for materials of the *p*-branches of thermoelectric generators intended for conversion of heat flux directly to electrical energy at high temperatures [1]. $Ca_3Co_4O_{9+\delta}$ has a monoclinic structure formed by alternating layers of $[Ca_2CoO_3]$ (NaCl structure) and $[CoO_2]$ (CdI_2 structure), which differ in period in one of the directions; for this reason, this compound is assigned to "misfit-layered phases" [2]. The use of the $Ca_3Co_4O_{9+\delta}$ ceramics synthesized by the conventional solid-phase method is limited because of their high porosity and, hence, low mechanical strength and low electrical conductivity.

An efficient way to obtain low-porosity $Ca_3Co_4O_{9+\delta}$ ceramics with improved thermoelectric characteristics is to use special sintering procedures, such as hot pressing [3–5] or spark plasma sintering [6–8]; however, such methods require quite rare and expensive equipment.

An alternative method to produce $Ca_3Co_4O_{9+\delta}$ ceramics with reduced porosity and, as a consequence, elevated electrical conductivity is two-step sintering [9–13]. In this case, at the first step, samples are sintered at high temperatures (1373–1473 K) exceeding the temperature of the peritectoid decomposition of the $Ca_3Co_4O_{9+\delta}$ phase (T_p = 1211 K in air [14]), and at the second step, to restore the phase composition of the ceramics, they are annealed for a long time in air or in an oxygen atmosphere at decreased temperatures (973–1173 K)[1].

One of the techniques to additionally improve the functional properties of $Ca_3Co_4O_{9+\delta}$ ceramics is to modify them with micro- and nanoparticles of metal

[1] Strictly speaking, as the $Ca_3Co_4O_{9+\delta}$ phase is heated, it initially undergoes a perictoid decomposition—by reaction P1: $Ca_3Co_4O_{9+\delta} \rightarrow Ca_3Co_2O_6$ + (Co, Ca)O (T_p = 1211 K in air [14]), and during subsequent heating, one of the products of reaction P1, the $Ca_3Co_2O_6$ phase, also decomposes by a perictoid reaction—reaction P2: $Ca_3Co_2O_6 \rightarrow$ (Ca, Co)O + (Co,Ca)O (T_p = 1312 K in air [14]).

oxides [15, 16], semiconductors [17], noble metals (Ag) [3, 18, 19], and transition metals (Fe, Co, Ni, Cu) [20–22] and also to create phase heterogeneity in them by their self-doping, i.e., using of the initial reaction mixture with the composition beyond the homogeneity region of the compound $Ca_3Co_4O_{9+\delta}$ [13, 23].

Such a modification of ceramics significantly increases their electrical conductivity σ [3, 16–19, 22] or Seebeck coefficient S [13, 23], and, as a result, improves such functional (thermoelectric) characteristics of the ceramics as the power factor $P = \sigma S^2$ and the dimensionless thermoelectric figure of merit $ZT = \sigma S^2 T/\lambda = PT/\lambda$, where T is absolute temperature.

The introduction of Fe, Co, or Ni particles to $Ca_3Co_4O_{9+\delta}$ [20, 21] considerably decreased the porosity of the ceramics, but did not lead to a essential improvement of their electrotransport and functional properties. We previously determined [22] that the addition of Cu nanoparticles to hot-pressed $Ca_3Co_4O_{9+\delta}$ ceramics substantially decreases their porosity and increases their electrical conductivity and power factor of the produced nanocomposites.

In this work, we studied the effect of the addition of copper particles on the microstructure, and electrotransport (electrical conductivity and Seebeck coefficient) and functional (power factor) properties of thermoelectric $Ca_3Co_4O_{9+\delta}$ ceramics obtained by two-step sintering.

EXPERIMENTAL

$Ca_3Co_4O_{9+\delta}$ ceramics were synthesized from analytically pure $CaCO_3$ and pure Co_3O_4, which were mixed in a stoichiometric ratio in a Fritsch Pulverisette 6.0 planetary mill (300 rpm, 30 min, ethanol added, grinding bowl and grinding balls made of ZrO_2), compacted into pellets 19 mm in diameter and 2–3 mm in height, and annealed in air for 12 h at 1173 K. To synthesize $Ca_3Co_4O_{9+\delta} + x$ wt % Cu ceramics (x = 3, 6, 9), the annealed samples were ground in an agate mortar and divided into four parts. To the last three parts, copper samples of necessary weights were added, after which the mixed samples were ground in the mill again and compacted into bars 5 × 5 × 30 mm. The bar-shaped samples were then sintered in air for 24 h at a temperature of 1173 K and 6 h at temperatures of 1273, 1373, and 1473 K, respectively. The samples sintered at T_{sint} = 1273–1473 K were additionally annealed in air at 1173 K for 71 h.

The theoretical density ρ_t of the samples was calculated from the formula

$$\rho_t = \omega_{349}\rho_{349} + \omega_{Cu}\rho_{Cu},$$

where ω_{349}, ω_{Cu} and ρ_{349}, ρ_{Cu} are the mass fractions of the components of the ceramics and their X-ray densities, respectively, the latter $Ca_3Co_4O_{9+\delta}$ and Cu being 4.68 [2] and 8.92 g/cm^3, respectively. The apparent density ρ_a of the ceramics was calculated from the geometric sizes and weights of the samples, and the porosity of the produced materials was found from the equation

$$\Pi = (1 - \rho_a/\rho_t) \times 100\%.$$

The samples were identified by X-ray powder diffraction analysis with a Bruker D8 ADVANCE X-ray diffractometer (CuK_α radiation) and IR absorption spectroscopy with a Thermo Nicolet NEXUS spectrometer. The microstructure of the samples was investigated by scanning electron microscopy with a JEOL JSM-5610 LV scanning electron microscope. The electrical conductivity of the sintered ceramics was measured at direct current ($I \le 50$ mA) by the four-point probe method (V7-58 and V7-53 digital voltmeters, B5-47 current source) in air in the temperature range 300–1100 K in dynamic mode at a heating and cooling rate of 3–5 deg/min with an error of $\delta(\sigma) \le \pm 5\%$. The Seebeck coefficient S of the sample was measured with respect to silver (with a V7-65/3 digital voltmeter) in air in the temperature range 300–1100 K with an error of $\delta(S) \le \pm 10\%$ at a temperature gradient between the hot and cold ends of the sample of about 20–25 K. Before measuring the electrophysical properties, Ag electrodes were formed on the surface of the sample by burning-in a silver paste at 1073 K for 15 min. The temperature was measured with chromel–alumel thermocouples. Electrotransport properties of the sintered ceramics were measured in the direction perpendicular to the pressing axis ($\sigma_\perp$, $S_\perp$), and the electrical conductivity was measured also in the direction parallel to the pressing axis ($\sigma_\parallel$, $S_\parallel \approx S_\perp$). The apparent activation energy E_A of the electrical conductivity of the samples was calculated from the linear parts of the $\ln(\sigma T) = f(T)$ curves.

RESULTS AND DISCUSSION

The sintering of the $Ca_3Co_4O_{9+\delta}$ + 9 wt % Cu sample at 1473 K led to significant melting of a surface layer and noticeable interaction of the sample with the material of the support, because of which we failed to study this sample.

The data in Table 1 shows that the porosity of the produced materials regularly decreases with increasing sintering temperature and also copper content of the samples (except the series sintered at 1473 K); it agrees well with the results of the recent works [20, 21], in which the same method was used to synthesize $Ca_3Co_4O_{9+\delta} + x$ vol % M (M = Co, Ni; x = 3, 6, 9) composite ceramics with reduced porosity.

After the final step of the synthesis, the $Ca_3Co_4O_{9+\delta}$ samples sintered at different temperatures were single-phase (within the error of X-ray powder diffraction analysis) and contained only the phase of layered calcium cobaltite [2] (Figs. 1a–1d, curve *1*). Along with the reflections of the $Ca_3Co_4O_{9+\delta}$ matrix phase, the

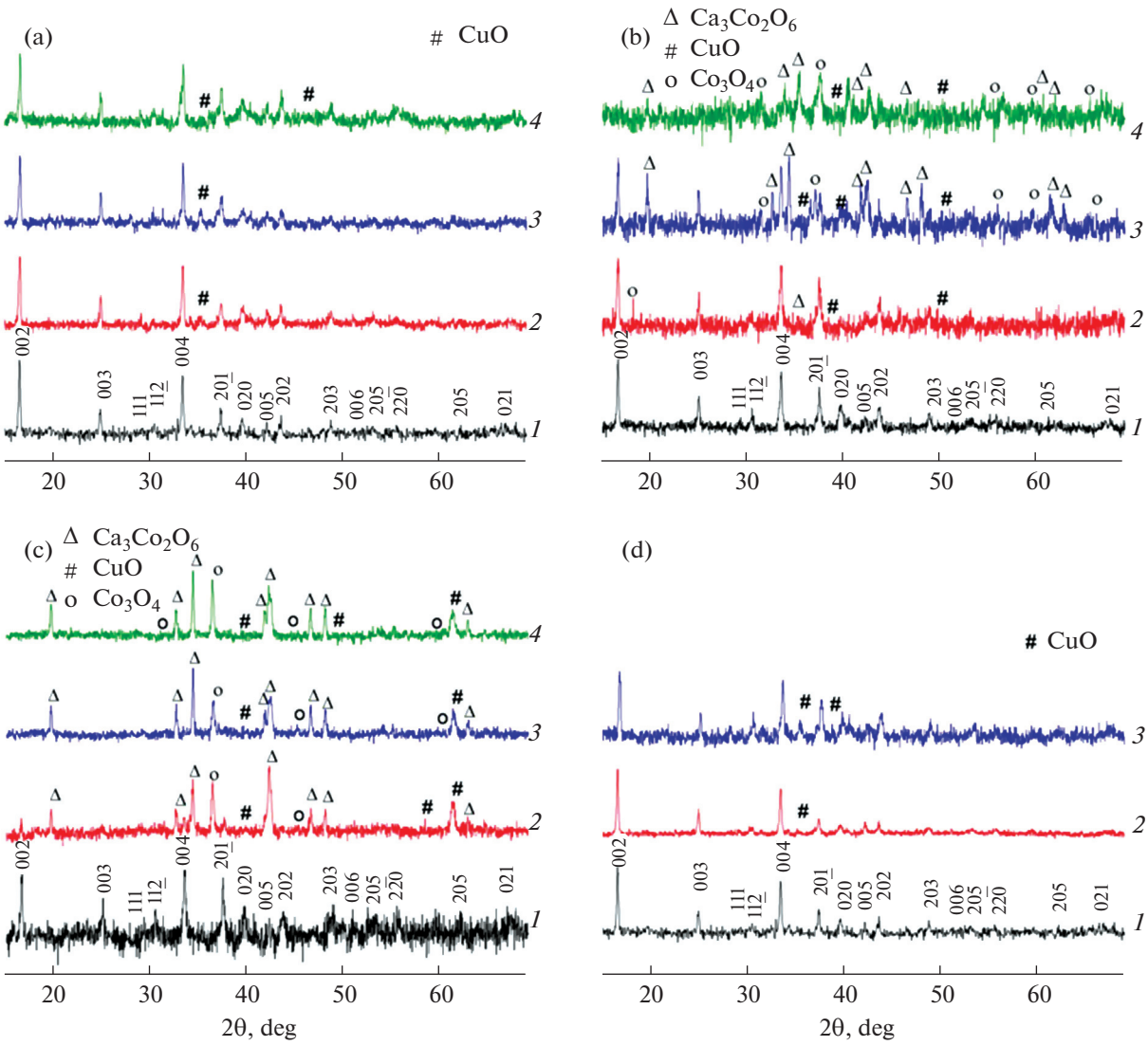

Fig. 1. X-ray powder diffraction patterns of the $Ca_3Co_4O_{9+\delta}$ + x wt % Cu composites sintered at (a) 1173, (b) 1273, (c) 1373, and (d) 1473 K (at x = (*1*) 0, (*2*) 3, (*3*) 6, and (*4*) 9). The numbers in pattern *1* are the Miller indices of the $Ca_3Co_4O_{9+\delta}$ phase.

X-ray powder diffraction patterns of the $Ca_3Co_4O_{9+\delta}$ + x wt % Cu powders show the reflections of copper oxide CuO (Figs. 1a–1d, curves *2–4*) formed by the oxidation of metallic copper by atmospheric oxygen[2], and the X-ray powder diffraction patterns of the samples sintered at 1273 and 1373 K also exhibit the reflections of the $Ca_3Co_2O_6$ phase, a product of the perictoid decomposition of layered calcium cobaltite [14], and cobalt oxide Co_3O_4. With increasing copper content of the $Ca_3Co_4O_{9+\delta}$ + x wt % Cu composites, the intensity of the reflections of the $Ca_3Co_2O_6$ and Co_3O_4 phases increases, and the intensity of the reflections of the $Ca_3Co_4O_{9+\delta}$ phase decreases (Figs. 1b, 1c). According to the X-ray powder diffraction data, in the $Ca_3Co_4O_{9+\delta}$ + 9 wt % Cu samples sintered at 1273 and 1373 K, and also in the $Ca_3Co_4O_{9+\delta}$ + 6 wt % Cu sample sintered at 1373 K, the $Ca_3Co_4O_{9+\delta}$ is practically absent. One of the possible causes of it can be the inhibition of peritectoid reaction P1 because of the presence of particles of the impurity phase CuO in the samples. Our results agree with the data of the works [20, 21] that the content of the $Ca_3Co_4O_{9+\delta}$ phase in the $Ca_3Co_4O_{9+\delta}$ + x vol % Co composites obtained by two-step sintering decreases with increasing x, and in the $Ca_3Co_4O_{9+\delta}$ + x vol % M (M = Fe, Ni) composites, this phase is absent.

[2] Copper(II) oxide formed by the oxidation of metallic copper (Cu) by atmospheric oxygen should be reduced in air at temperatures above 1273 K to Cu_2O (cuprite) by the reaction $CuO \rightarrow Cu_2O + 1/2O_2$ [24]. As a result of the long-term annealing of the ceramics in air at 1173 K, the reverse reaction occurs, and copper oxide in the ceramics should exist as tenorite (CuO).

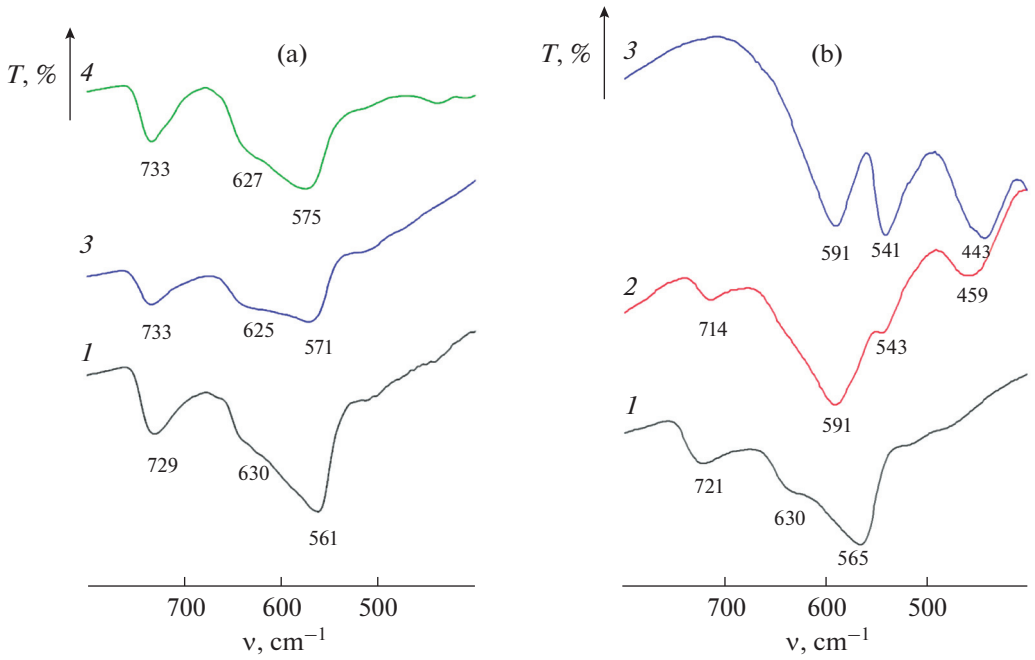

Fig. 2. IR absorption spectra of the (a) $Ca_3Co_4O_{9+\delta}$ and (b) $Ca_3Co_4O_{9+\delta}$ + 9 wt % Cu samples sintered at (*1*) 1173, (*2*) 1273, (*3*) 1373, and (*4*) 1473 K.

The IR absorption spectra of the $Ca_3Co_4O_{9+\delta}$ powders with different thermal history (Fig. 2a) contain three pronounced absorption bands with extrema at 561–575 cm^{-1} (ν_1), 625–630 cm^{-1} (ν_2), and 729–733 cm^{-1} (ν_3), which correspond [25] to the stretching vibrations of the Co–O (ν_1 and ν_2) and Ca–O (ν_3) bonds in the structure of the $Ca_3Co_4O_{9+\delta}$ phase. Along with the absorption bands of the $Ca_3Co_4O_{9+\delta}$ matrix phase (565 cm^{-1} (ν_1), 630 cm^{-1} (ν_2), and 714–721 cm^{-1} (ν_3)), the IR absorption spectra of the $Ca_3Co_4O_{9+\delta}$ + 9 wt % Cu composite also presents additional absorption bands with extrema at 443–459 cm^{-1} (ν_4), 541–543 cm^{-1} (ν_5), and 591 cm^{-1} (ν_6), which characterize the stretching vibrations of the Cu–O bonds (ν_4 and ν_5) in copper(II) oxide [26], and also the stretching vibrations of the Ca–O bonds (ν_6) in the structure of the $Ca_3Co_2O_6$ phase [27].

As is seen from the scanning electron microscopy data (Fig. 3), the ceramics synthesized in this work has a microstructure that is typical of layered calcium cobaltite and comprises highly anisotropic plates (grains), the size of which increases with increasing copper content of the samples from ~3–7 μm for $Ca_3Co_4O_{9+\delta}$ to ~10–15 μm for the $Ca_3Co_4O_{9+\delta}$ + 9 wt % Cu composite material, with the thickness being ~0.5–1 μm (Figs. 3a–3d). Hence, it follows that the introduction of copper particles to the $Ca_3Co_4O_{9+\delta}$ ceramics with subsequent two-step sintering gives coarser-grained ceramics. Interestingly, the modification of the hot-pressed $Ca_3Co_4O_{9+\delta}$ ceramics with copper nanoparticles gave the opposite result, namely, a decrease in the grain size of the ceramics [22]. The plate size of the ceramics increased with increasing its sintering temperature from ~2–5 μm for the $Ca_3Co_4O_{9+\delta}$ + 3 wt % Cu sample sintered at 1173 K to ~5–10 μm for the material that had the same composition but was sintered at higher temperatures (1273–1473 K) (Figs. 3e–3h), and the most crystallized grains were found in the ceramics sintered at 1273 and 1373 K.

The electrical conduction of the $Ca_3Co_4O_{9+\delta}$ + x wt % Cu (x = 6, 9) samples sintered at 1373 K is of the semiconductor type ($\partial\sigma/\partial T > 0$) throughout the studied temperature range, whereas the dependence $\sigma = f(T)$ for all the other tested materials is submetallic ($\partial\sigma/\partial T < 0$) near room temperature and becomes to be of the semiconductor type near 400–500 K (Figs. 4a, 4d, 4g, 4j), which is due to the metal–semiconductor phase transition occurring in layered calcium cobaltite in this temperature range [28]. An increase in the sintering temperature of the $Ca_3Co_4O_{9+\delta}$ ceramics leads to a regular increase in its electrical conductivity due to a decrease in the porosity, whereas the dependence of σ of the $Ca_3Co_4O_{9+\delta}$ + x wt % Cu composites on their thermal history and composition is complex (Figs. 4a, 4d, 4g, 4j; Table 1). The electrical conductivity of the $Ca_3Co_4O_{9+\delta}$ + x wt % Cu samples sintered at 1173 K, and also the $Ca_3Co_4O_{9+\delta}$ + 3 wt % Cu material sintered at 1273 K (with the maximum electrical conductivity $\sigma_{\perp,1100}$ = 82.2 S/cm (Table 1)) is higher than that of the $Ca_3Co_4O_{9+\delta}$ matrix phase owing to the

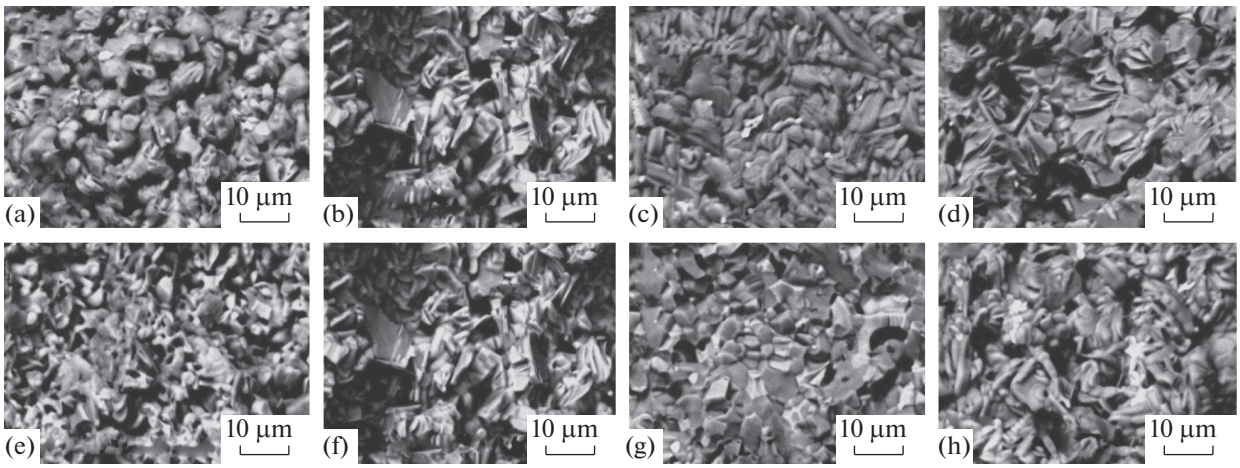

Fig. 3. Electron micrographs of the cleaved surfaces of the $Ca_3Co_4O_{9+\delta}$ + *x* wt % Cu ceramics sintered at 1273 K (*x* = (a) 0, (b) 3, (c) 6, and (d) 9) and the $Ca_3Co_4O_{9+\delta}$ + 3 wt % Cu composite sintered at (e) 1173, (f) 1273, (g) 1373, and (h) 1473 K.

improvement of the sinterability of the samples modified with copper particles. The other composites are far below in σ to the matrix phase with the same thermal history because the former contain low-conductive phases of copper(II) oxide (formed by the oxidation of metallic copper by atmospheric oxygen), and $Ca_3Co_2O_6$ and Co_3O_4 [13, 29]; the electrical conductivity is lowest for the $Ca_3Co_4O_{9+\delta}$ + *x* wt % Cu ceramics sintered at 1373 K (Fig. 4g), which contains the maximum amount of these phases.

$Ca_3Co_4O_{9+\delta}$ single crystals are known to have strong anisotropy of the electrical conductivity, which in the *ab* plane (in the direction of the $[CoO_2]$ layers, σ_{ab}) is hundreds of times higher than that in the direction perpendicular to this plane (to the $[CoO_2]$ layers, σ_c) [30]. The $Ca_3Co_4O_{9+\delta}$ + *x* wt % Cu polycrystalline ceramics that we synthesized also has marked anisotropy of the electrical conductivity, which in the direction perpendicular to the pressing axis ($\sigma_\perp$) in the samples containing insignificant amounts of low-conductive phases ($Ca_3Co_2O_6$, Co_3O_4, CuO) is noticeably higher than that in the direction parallel to the pressing axis ($\sigma_\parallel$; in the materials sintered at 1173 K, by 35–65%) (Figs. 4a, 4d, 4g, 4j). This is likely to be due to partial texturing of the ceramics (alignment of grains of the $Ca_3Co_4O_{9+\delta}$ grains in the direction parallel to the pressing axis) [6].

The activation energy of the electrical conductivity of the samples that was calculated in the temperature range 700–1100 K varies within the range 0.086–0.117 eV (except the $Ca_3Co_4O_{9+\delta}$ + *x* wt % Cu composites sintered at 1373 K and the $Ca_3Co_4O_{9+\delta}$ + 3 wt % Cu material sintered at 1473 K, Table 1). This is close to the published [13, 20–22, 28] values for $Ca_3Co_4O_{9+\delta}$ composites and suggests a common mechanism of electrical conductivity, which is determined by the charge transfer in the matrix phase, layered calcium cobaltite.

The sign of the Seebeck coefficient for all the studied materials is positive ($S > 0$), whence it follows that the majority carriers in them are holes and the materi-

Table 1. Theoretical density ρ_t (g/cm^3), apparent density ρ_a (g/cm^3), porosity Π (%), electrotransport parameters ($E_{A,\perp}$, $E_{A,\parallel}$, meV), and thermoelectric characteristics ($\sigma_{1100,\perp}$, S/cm; $S_{1100,\perp}$, μV/K; $P_{1100,\perp}$, μW/(m K^2)) of the $Ca_3Co_4O_{9+\delta}$ + *x* wt % Cu composites sintered at various temperatures (T_{sint}, K)

x	ρ_t	ρ_a	Π	$E_{A,\perp}$	$E_{A,\parallel}$	$\sigma_{1100,\perp}$	$S_{1100,\perp}$	$P_{1100,\perp}$
T_{sint} = 1173 K								
0	4.68	2.86	38.9	117	112	36.9	200	148
3	4.80	3.03	36.9	92.8	93.6	45.6	179	146
6	4.92	3.20	35.0	94.8	108	54.6	186	189
9	5.03	3.39	32.6	96.1	111	52.7	175	161
T_{sint} = 1273 K								
0	4.68	3.31	29.3	86.4	76.1	43.2	183	145
3	4.80	3.86	19.6	97.7	114	82.2	202	335
6	4.92	4.14	15.9	94.8	108	41.1	188	145
9	5.03	4.26	15.3	96.1	111	53.1	175	162
T_{sint} = 1373 K								
0	4.68	3.92	16.2	115	92.6	64.8	183	217
3	4.80	4.33	9.8	159	204	12.2	219	58.5
6	4.92	4.46	9.3	308	304	16.7	202	49.8
9	5.03	4.52	10.1	334	362	12.0	170	34.7
T_{sint} = 1473 K								
0	4.68	4.04	13.7	95.4	81.9	74.8	200	299
3	4.80	3.48	27.5	159	204	55.1	200	220
6	4.92	3.51	28.7	103	107	62.2	197	241

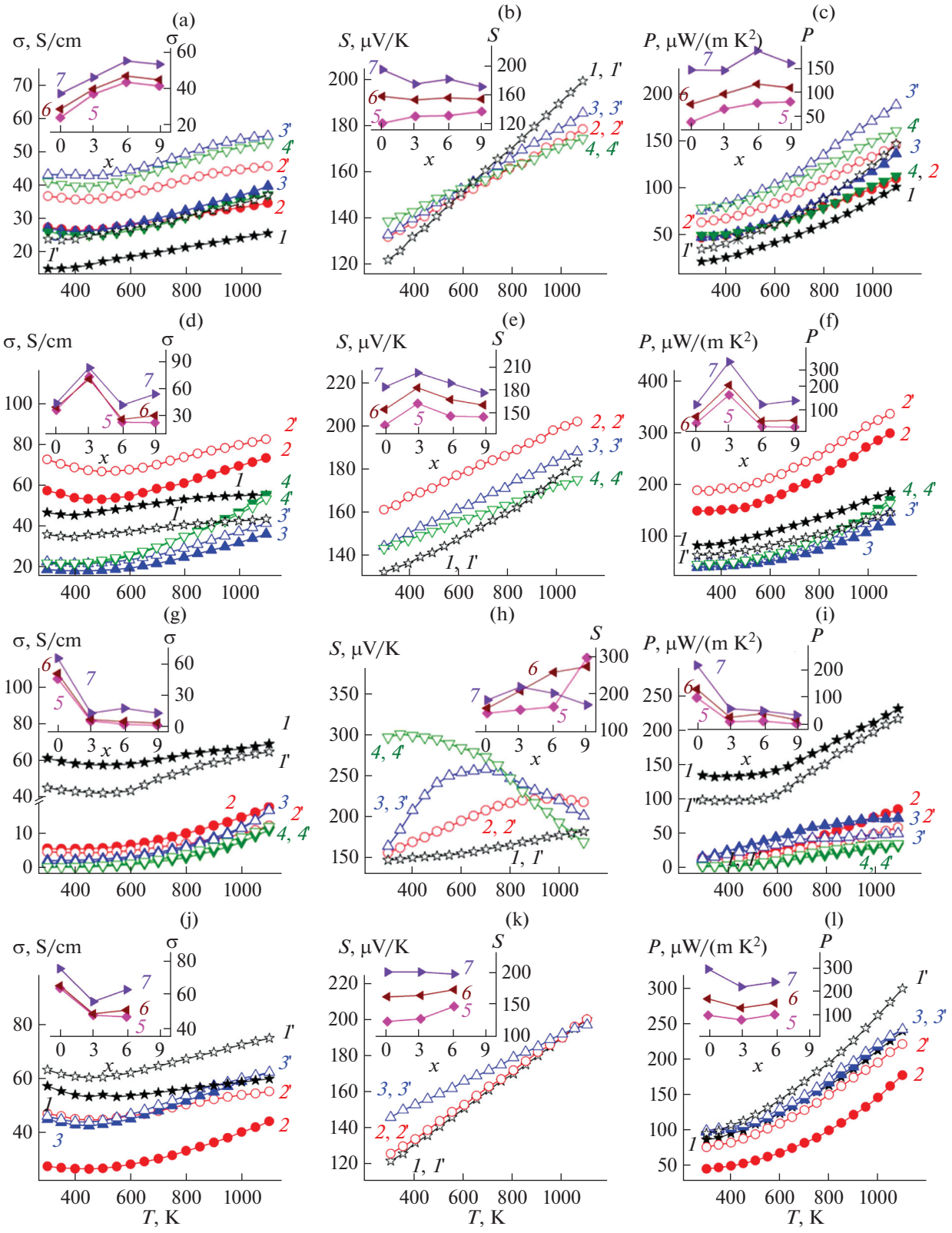

Fig. 4. Temperature dependences of the (a, d, g, j) electrical conductivity, (b, e, h, k) Seebeck coefficient, and (c, f, i, l) power factor of the $Ca_3Co_4O_{9+\delta}$ + *x* wt % Cu composites sintered at (a–c) 1173, (d–f) 1273, (g–i) 1373, and (j–l) 1473 K in the direction (*1*–*4*) parallel and (*1*′–*4*′) perpendicular to the pressing axis at *x* = (*1*, *1*′) 0, (*2*, *2*′) 3, (*3*, *3*′) 6, and (*4*, *4*′) 9. The insets illustrate the concentration dependences of the (a, d, g, j) electrical conductivity, (b, e, h, k) Seebeck coefficient, and (c, f, i, l) power factor of the ceramics in the direction perpendicular to the pressing axis at *T* = (*5*) 300, (*6*) 700, and (*7*) 1100 K.

als are *p*-type semiconductors. *S* monotonically increases with increasing temperature (except for the $Ca_3Co_4O_{9+\delta} + x$ wt % Cu composites sintered at 1373 K, for which the dependence $S = f(T)$ is extremal), varying within the range 120–200 μV/K (Figs. 4b, 4e, 4h, 4k; Table 1), which is characteristic of $Ca_3Co_4O_{9+\delta}$ ceramics [3–13, 22, 27]. *S* of the $Ca_3Co_4O_{9+\delta} + x$ wt % Cu composites is typically higher than that of the $Ca_3Co_4O_{9+\delta}$ matrix samples, which is due to the phase heterogeneity of the composites [5, 13, 22, 23]. The elevated values of the Seebeck coefficient for the $Ca_3Co_4O_{9+\delta} + x$ wt % Cu composites sintered at 1373 K and the observed anomalous dependence $S = f(T)$ are probably caused by the Co_3O_4 phase, which is contained in them in significant amounts and is characterized by high *S* values and by its anomalous temperature dependence [29].

The power factor increases with temperature, and for the $Ca_3Co_4O_{9+\delta} + x$ wt % Cu materials sintered at 1173 K, with increasing *x* (Figs. 4c, 4f, 4i, 4l). *P* is maximum for the $Ca_3Co_4O_{9+\delta}$ + 3 wt % Cu sample sintered at 1273 K and is 335 μW/(m K^2) at 1100 K, which is by a factor of 2.3 higher than the power factor of the copper-unmodified $Ca_3Co_4O_{9+\delta}$ ceramic with the same thermal history ($P_{\perp,1100} = 145$ μW/(m K^2)) and is by a factor of 33 higher than that for the high-porosity $Ca_3Co_4O_{9+\delta}$ ceramic synthesized by the conventional solid-phase method ($P_{1100} \sim 100$ μW/(m K^2)) [31, 32]. The high power factor of the $Ca_3Co_4O_{9+\delta} + 3$ wt % Cu composite ceramic sintered at 1273 K is due to the simultaneously increased values of its electrical conductivity (because of the decreased porosity) and its Seebeck coefficient (probably because of the phase heterogeneity of the material). A little inferior in *P* to this material is the $Ca_3Co_4O_{9+\delta}$ ceramic sintered at 1473 K, for which the power factor at 1100 K is 299 μW/(m K^2).

CONCLUSIONS

Composite thermoelectric $Ca_3Co_4O_{9+\delta}$-based materials doped with copper particles were synthesized by two-step sintering; their phase composition was determined; and their microstructure, electrotransport properties (electrical conductivity and Seebeck coefficient), and thermoelectric properties (power factor) were studied. The effect of the sintering temperature (thermal history) and the addition of copper particles on the physicochemical and functional properties of the ceramics was analyzed. It was determined that the introduction of copper particles to the ceramics improves their sinterability at moderate sintering temperatures ($T_{sint} \le 1273$ K), leading to a decrease in the porosity of the samples and an increase in their electrical conductivity and power factor. At the same time, the oxidation of copper to less conductive copper(II) oxide decreases the electrical conductivity and power factor of the ceramics sintered at elevated temperatures ($T_{sint} \ge 1373$ K). The power factor is maximum for the $Ca_3Co_4O_{9+\delta}$ + 3 wt % Cu material sintered at 1273 K (335 μW/(m K^2) at a temperature of 1100 K), which is by a factor of 2.3 higher than the power factor of the copper-free $Ca_3Co_4O_{9+\delta}$ sample with the same thermal history (145 μW/(m K^2) at 1100 K), by a factor of 3.3 higher than the power factor of the $Ca_3Co_4O_{9+\delta}$ ceramic synthesized by the conventional solid-phase method, and 10% higher than the power factor of the unmodified $Ca_3Co_4O_{9+\delta}$ ceramic sintered at 1473 K (299 μW/(m K^2) at 1100 K). Thus, the modification of $Ca_3Co_4O_{9+\delta}$ with copper particles enables one to produce thermoelectric ceramics with improved characteristics by two-step sintering in which the sintering temperature is reduced (by 200 K) in comparison with the conventionally used sintering temperature: 1273 K (with one peritectoid decomposition by reaction P1) instead of 1473 K (with two peritectoid decompositions by reactions P1 and P2).

FUNDING

This work was supported by the State Program of Scientific Research "Physical Materials Science and New Materials and Technologies," Subprogram "Materials Science and Materials Technologies," Task 1.55 "Research and Design of Composite Thermoelectric Materials Based on Layered Calcium Cobaltite."

CONFLICT OF INTEREST

The authors declare that they have no conflicts of interest.

REFERENCES

1. *Oxide Thermoelectrics. Research Signpost*, Ed. by K. Koumoto, I. Terasaki, and N. Murayama (Trivandrum, Research Signpost, India, 2002).

2. A. C. Masset, C. Michel, A. Maignan, et al., Phys. Rev. **62**, 166 (2000). https://doi.org/10.1103/PhysRevB.62.166
3. P.-H. Xiang, Y. Kinemuchi, H. Kaga, et al., J. Alloys Compd. **454**, 364 (2008). https://doi.org/10.1016/j.jallcom.2006.12.102
4. S. Katsuyama, Y. Takiguchi, and M. Ito, J. Mater. Sci. **43**, 3553 (2008). https://doi.org/10.1007/s10853-008-2561-x
5. A. I. Klyndyuk, I. V. Matsukevich, M. Janek, et al., Russ. J. Appl. Chem. **93**, 1126 (2020). https://doi.org/10.1134/S1070427220080030
6. N. Y. Wu, T. C. Holgate, N. V. Nong, et al., J. Eur. Ceram. Soc. **34**, 925 (2014). https://doi.org/10.1016/j.jeurceramsoc.2013.10.022
7. A. K. Krolicka, M. Piersa, A. Mirowska, et al., Ceram. Int. **44**, 13736 (2018). https://doi.org/10.1016/j,ceramint.2018.04.215
8. N. Kanas, S. P. Singh, M. Rotan, et al., J. Eur. Ceram. Soc. **38**, 1592 (2018). https://doi.org/10.1016/j.jeurceramsoc.2017.11.011
9. M. A. Madre, F. M. Costa, N. M. Ferreira, et al., J. Eur. Ceram. Soc. **33**, 1747 (2013). https://doi.org/10.1016/j.jeurceramsoc.2013.01.029
10. M.-G. Kang, K.-H. Cho, J.-S. Kim, et al., Acta Mater. **73**, 251 (2014). https://doi.org//10.1016/j.actamat.2014.04.008
11. T. Schulz and J. Töpfer, J. Alloys Compd. **659**, 122 (2016). https://doi.org/10.1016/j.jallcom.2015.11.001
12. Z. Shi, J. Xu, J. Zhu, et al., J. Mater. Sci.: Mater. Electron. **31**, 2938 (2020). https://doi.org/10.1007/s10854-019-02838-0
13. A. I. Klyndyuk, E. A. Chizhova, E. A. Tugova, et al., Glass Phys. Chem. **46**, 548 (2020). https://doi.org/10.1134/S1087659620060127
14. D. Sedmidubsky, V. Jakes, O. Jankovsky, et al., J. Solid State Chem. **194**, 199 (2012). https://doi.org/10.1016/j.jssc.2012.05.014
15. F. Delorme, P. Diaz-Chao, E. Guilmeau, et al., Ceram. Int. **41**, 10038 (2015). https://doi.org/10.1016/j.ceramint.2015.04.091
16. R. K. Gupta, R. Sharma, A. K. Mahapatro, et al., Physica B. **483**, 48 (2016). https://doi.org/10.1016/j.physb.2015.12.028
17. H. Amaveda, M. Mora, O. J. Dura, et al., J. Eur. Ceram. Soc. **41**, 402 (2021). https://doi.org/10.1016/j.jeurceramsoc.2020.08.024
18. F. Kahraman, M. A. Madre, Sh. Rasekh, et al., J. Eur. Ceram. Soc. **35**, 3835 (2015). https://doi.org/10.1016/j.jeyrceramsoc.2015.05.029
19. Z. Shi, F. Gao, J. Xu, et al., J. Eur. Ceram. Soc. **39**, 3086 (2019). https://doi.org/10.1016/j.jeurceramsoc.2019.04.004
20. G. Constantinescu, A. R. Sarabando, Sh. Rasekh, et al., Materials **13**, 1060 (2020). https://doi.org/10.3390/ma13051060
21. G. Constantinescu, S. M. Mikhalev, A. D. Lisenkov, et al., Materials **14**, 980 (2021). https://doi.org/10.3390/ma14040980
22. A. I. Klyndyuk, I. V. Matsukevich, M. Janek, et al., Inorg. Mater. **56**, 1263 (2020). https://doi.org/10.1134/S0020168520110059
23. X.-D. Zhou, L. R. Pederson, E. Thomsen, et al., Electrochem. Solid-State Lett. **12**, F1 (2009). https://doi.org/10.1149/1.3039948
24. L. Schramm, G. Behr, W. Löser, et al., J. Phase Equilib. Diffus. **26**, 605 (2005). https://doi.org/10.1361/154770305X74421
25. Y. Zhang and J. Zhang, J. Mater. Process. Technol. **208**, 70 (2008). https://doi.org/10.1016/j.jmatprotec.2007.12.093
26. Y. C. Zhang, J. Y. Tang, G. L. Wang, et al., J. Cryst. Growth. **294**, 278 (2006). https://doi.org/10.1016/j.jcrysgro.2006.06.038
27. D. Lu, G. Chen, J. Pei, et al., J. Rare Earths. **26**, 168 (2008). https://doi.org/10.1016/S1002–0721(08)60059–9
28. Y.-H. Lin, J. Lan, Z. Shen, et al., Appl. Phys. Lett. **94**, 072107 (2009). https://doi.org/10.1063/1.308687
29. A. I. Klyndyuk, N. S. Krasutskaya, and E. A. Chizhova, Glass Phys. Chem. **44**, 100 (2018). https://doi.org/10.1134/S1087659618020086
30. S. Bresh, B. Mieller, D. Schoenauer-Kamin, et al., J. Am. Ceram. Soc. **104**, 917 (2020). https://doi.org/10.1111/jace.17541
31. M. Tahashi, K. Ogawa, M. Takahashi, et al., J. Ceram. Soc. Jpn. **121**, 444 (2013).
32. I. V. Matsukevich, A. I. Klyndyuk, E. A. Tugova, et al., Russ. J. Appl. Chem. **88**, 1241 (2015). https://doi.org/10.1134/S1070427215080030

Translated by V. Glyanchenko